BBA - Biomembranes 1860 (2018) 2436–2445

Contents lists available at ScienceDirect

BBA - Biomembranes

journal homepage: www.elsevier.com/locate/bbamem

How to minimize dye-induced perturbations while studying biomembrane structure and dynamics: PEG linkers as a rational alternative

Edouard Mobarak[a,b], Matti Javanainen[a,b,c], Waldemar Kulig[a,b], Alf Honigmann[d], Erdinc Sezgin[e], Noora Aho[a], Christian Eggeling[e,f,g], Tomasz Rog[a,b], Ilpo Vattulainen[a,b,h,*]

[a] Department of Physics, University of Helsinki, P. O. Box 64, FI-00014 Helsinki, Finland
[b] Laboratory of Physics, Tampere University of Technology, P. O. Box 692, FI-33101 Tampere, Finland
[c] Institute of Organic Chemistry and Biochemistry, Academy of Sciences of the Czech Republic, Prague, Czech Republic
[d] Max Planck Institute of Molecular Cell Biology and Genetics, Pfotenhauerstr. 108, 01307 Dresden, Germany
[e] MRC Human Immunology Unit, Weatherall Institute of Molecular Medicine, University of Oxford, Headley Way, OX3 9DS Oxford, United Kingdom
[f] Institute of Applied Optics Friedrich–Schiller–University Jena, Max-Wien Platz 4, 07743 Jena, Germany
[g] Leibniz Institute of Photonic Technology e.V., Albert-Einstein-Straße 9, 07745 Jena, Germany
[h] MEMPHYS - Center for Biomembrane Physics (www.memphys.dk)

ARTICLE INFO

Keywords:
Fluorescent probe
PEG linker
Lipid membrane
Atomistic simulation
Molecular dynamics simulation
Super-resolution microscopy

ABSTRACT

Organic dye-tagged lipid analogs are essential for many fluorescence-based investigations of complex membrane structures, especially when using advanced microscopy approaches. However, lipid analogs may interfere with membrane structure and dynamics, and it is not obvious that the properties of lipid analogs would match those of non-labeled host lipids. In this work, we bridged atomistic simulations with super-resolution imaging experiments and biomimetic membranes to assess the performance of commonly used sphingomyelin-based lipid analogs. The objective was to compare, on equal footing, the relative strengths and weaknesses of acyl chain labeling, headgroup labeling, and labeling based on poly-ethyl-glycol (PEG) linkers in determining biomembrane properties. We observed that the most appropriate strategy to minimize dye-induced membrane perturbations and to allow consideration of Brownian-like diffusion in liquid-ordered membrane environments is to decouple the dye from a membrane by a PEG linker attached to a lipid headgroup. Yet, while the use of PEG linkers may sound a rational and even an obvious approach to explore membrane dynamics, the results also suggest that the dyes exploiting PEG linkers interfere with molecular interactions and their dynamics. Overall, the results highlight the great care needed when using fluorescent lipid analogs, in particular accurate controls.

1. Introduction

There is increasing proof that cellular signaling is modulated and highly dependent on heterogeneous lateral organization of the plasma membrane [1–3]. Such heterogeneity is multi-fold, including a variety of distinct sub-compartments that differ in their biophysical properties and composition [2]. A specific physicochemical principle for a subtype of such lateral membrane heterogeneity was formalized within the membrane raft hypothesis, involving the preferential associations between cholesterol and saturated lipids that drive the formation of relatively packed (or ordered) membrane domains, and that selectively recruit certain lipids and proteins and compartmentalize cellular processes [2, 4]. A large number of studies have focused on understanding the basis of this heterogeneity and its physiological relevance [5]. Yet, it has appeared that techniques for observing such heterogeneity require strong specificity and high spatio-temporal resolution, since the involved sub-compartments are indeed distinct, appear on very small spatial scales, and are transient. Fluorescence labeling introduces such specificity, and the recent advent of fluorescence-based super-resolution microscopy methods delivers experimental approaches, such as the combination of Fluorescence Correlation Spectroscopy (FCS) with super-resolution Stimulated Emission Depletion (STED) microscopy (STED-FCS) [6], that feature high enough spatial and temporal resolution to decipher heterogeneity in the spatio-temporal dynamics of specific molecules [7, 8]. For example, using fluorescent analogs of specific lipids (i.e., saturated and unsaturated forms of phosphoethanolamine, sphingomyelin (SM), or gangliosides tagged with an organic dye), STED-FCS observations of the diffusion dynamics of these fluorescent lipid analogs revealed transient interactions with other slowly moving entities in systems with cholesterol, and including actin

* Corresponding author.
E-mail address: Ilpo.Vattulainen@helsinki.fi (I. Vattulainen).

https://doi.org/10.1016/j.bbamem.2018.07.003
Received 22 March 2018; Received in revised form 3 July 2018; Accepted 9 July 2018
Available online 18 July 2018

dependencies for sphingolipids but less for gangliosides [9–12].

Unfortunately, the dye label may influence the characteristics of the host lipid, changing its properties compared to the native form, especially with regard to properties such as size, polarity, and/or charge. While intensive controls on label type and position have revealed hardly any dependence of the label on the STED-FCS based observations of live-cell dynamics (in contrast to changes in lipid structure) [13], the controls have indicated a strong influence of the label on the ability to enter more ordered membrane regions (i.e., lipid-raft like sub-compartments): partitioning into ordered membrane environments changed with lipid type, dye label, and position [14–17], and reached levels as expected for the respective endogenous lipid counterpart only when introducing a spacer in form of a poly-ethyl-glycol (PEG) linker in-between the dye and the lipid [18]. However, the exact molecular mechanisms and conformations ruling these partitioning characteristics are not at all understood so far.

Molecular dynamics (MD) simulations have been extensively useful to study the behavior of molecular probes in lipid bilayers in terms of probe location, orientation, dynamics, and effects of the probes on the surrounding lipids and bulk bilayer properties [19–25]. These studies have provided compelling evidence that probe-induced perturbations in membrane structure and dynamics are of very short range, meaning that the probes typically have a significant effect up to ~2 nm from the probe in the membrane plane. The simulation studies have also explored lipid-label constructs, e.g., BODIPY-labeled GM1 [26], phosphatidylcholine [27], and cholesterol [28], and these studies have shown how the labeling interferes with, e.g., the host lipids' structure and partitioning. However, effects of lipid PEGylation on bilayer properties as well as effects arising from dye labels usually employed in advanced microscopy have not received similar attention yet; previous work based on MD simulations is summarized in a recent review [29].

Here we used atomistic MD simulations together with super-resolution microscopy [30] and biomimetic membrane systems to unravel the properties of several dye labels commonly used for super-resolution microscopy of biomembranes (ATTO647N, ATTO532, and Abberior Star Red (KK114)) in ordered and disordered membrane environments using fluorescent sphingomyelin-based analogs as the basis. To our knowledge, the approach of bridging super-resolution microscopy with atomistic simulations has not been used previously to explore how dyes interfere with membrane structure and dynamics, yet it is a very appealing approach since it combines atomistic and large-scale dynamics in a coherent fashion. The objective in our work was to compare the relative strengths and weaknesses of the above lipid analogs depending on whether the labeling was applied to a lipid acyl chain, lipid headgroup, or whether the labeling was based on a PEG chain linking the dye to the host lipid's headgroup. Of key interest studied in this work was the extent of dye-induced perturbations. Perhaps surprisingly, the suitability of PEG linkers to explore membrane properties with commonly used dyes (such as ATTO647N, ATTO532, and KK114) has been studied very little as yet, and also the possible drawbacks of PEG linkers have not been investigated much. Given that the use of PEG linkers sounds a rational approach, in this paper our aim is to shed light on the effects of the linkers in particular.

Our simulation results demonstrate that membrane perturbations due to the dyes are stronger in membranes that are in the liquid-ordered (L_o) phase than in more fluid bilayers that are in the liquid-disordered (L_d) phase, and that acyl-chain linked dyes induce stronger perturbations than headgroup-linked analogs. Further, the simulations correlate the positioning of the dye at the membrane-water interface with the experimentally measured partitioning characteristics of the lipid analog. This feature is most evident in L_o membranes, where the only SM-based analog favoring the L_o phase was found to be based on a PEG linker attaching the dye to the headgroup of its host sphingolipid. Our simulations revealed that the dye with the PEG linker resides mainly in the water phase, and that this arrangement of using a PEG linker also results in the weakest dye-induced membrane alterations. Surprisingly, we also found that the PEG linker changed the sub-diffusion characteristics of the SM analogs explored in our STED-FCS measurements. Analysis of the diffusion of the PEG-linked SM analog showed only minor signatures of interaction with immobile membrane constituents compared to probes without the PEG linker. This finding indicates two things: First, the trap-diffusion characteristics of SM analogs are independent of partitioning characteristics between ordered/disordered domains in the plasma membrane. Second, the PEG linker may shield the probe to become integrated into dense protein clusters (diffusion traps).

The results of the atomistic MD simulations were observed to be in line with experimental data measured in giant plasma membrane vesicles (GPMVs), showing the preference of these lipid analogs for ordered and disordered membrane environments and also their diffusion modes in living cell membranes as probed by STED-FCS, giving insights into the molecular mechanisms and conformations ruling the different biasing partitioning and diffusion characteristics of the sphingolipid analogs.

Our results highlight that PEG linkers are a promising approach for exploring membrane structure and dynamics, however our study also highlights the great care needed when using fluorescent lipid analogs and interpreting their results, in particular accurate controls [9, 30, 31].

2. Results

2.1. Lipid analogs whose features were assessed through both atomistic simulations and experiments included a number of commonly used probes

In atomistic MD simulations, we considered several fluorescent sphingolipid analogs (abbreviated here as SM), similar to those employed in previous experimental studies [9–14, 18]. The organic dyes ATTO647N, ATTO532, and/or Abberior Star Red (KK114) were attached to either the headgroup of ceramide phosphoethanolamine d17:1/12:0 (HEAD), or the acyl chain of sphingomyelin d18:1/2:0 (TAIL). In addition, KK114 was also attached to the ceramide phosphoethanolamine headgroup via a short 10 or 50 unit long PEG linker (HEAD–PEG10 or HEAD–PEG50) [11, 18]. All the host lipids were therefore based on the ceramide structure and are expected to mimic the behavior of SM-like lipids. In addition, we considered two differently ordered membrane bilayers into which the lipid analogs were embedded: a disordered membrane (liquid-disordered, L_d) made up of unlabeled di-oleoyl-phosphatidylcholine (DOPC), and a more ordered membrane (liquid-ordered, L_o) made up of 33 mol% cholesterol and 67 mol% SM d18:1/16:0 (all unlabeled). Given these choices, we studied the lipid analogs as 8 different scenarios with the dye attached to the headgroup (HEAD-L_o, HEAD-L_d, HEAD-PEG10-L_o, HEAD-PEG10-L_d, HEAD-PEG50-L_o, HEAD-PEG50-L_d) or to an acyl chain (TAIL-L_o, TAIL-L_d), with three different dyes (Table 1). Fig. 1 summarizes the chemical structures of the dyes and the lipids used in this study.

The properties of the dyes differ quite significantly. ATTO647N is a highly hydrophobic dye. It features positively charged aromatic nitrogen atoms whose charge is delocalized over a few neighboring atoms, but this does not change the overall hydrophobic nature of the dye. Meanwhile, ATTO532 is a highly polar label due to the presence of two negatively charged sulfate groups and the polar amide and ether groups. KK114 is also a highly polar dye due to three charged groups: two negative and one positive.

Details on the molecular parameterization as well as calculation algorithms used in the simulation models are given in the Materials and Methods section. Considering all the different SM analogs and the L_d and L_o membrane environments, we in total simulated 14 different systems (each over a period of 400 ns) as listed in Table 1. Every system was simulated as three independent replicas. Finally, the simulations were complemented with super-resolution imaging experiments and biomimetic membranes: details are discussed in the Materials and methods section.

Table 1
Summary of the studied lipid bilayers. L_d stands for liquid-disordered and L_o for liquid-ordered. HEAD (TAIL) refers to headgroup (acyl-chain) labeling. The structures of the dyes are given in Fig. 1. The estimated errors in the area per lipid (APL) are < 0.003 nm^2 for all systems. Standard errors were calculated through the method described elsewhere [55].

System	Dye	Attached to	Bilayer phase	Area per lipid [nm^2]
1	ATTO647N	HEAD	L_d	0.740
2	ATTO647N	HEAD	L_o	0.416
3	ATTO647N	TAIL	L_d	0.740
4	ATTO647N	TAIL	L_o	0.419
5	ATTO532	HEAD	L_d	0.725
6	ATTO532	HEAD	L_o	0.398
7	ATTO532	TAIL	L_d	0.715
8	ATTO532	TAIL	L_o	0.409
9	KK114	HEAD	L_d	0.690
10	KK114	HEAD	L_o	0.400
11	KK114	HEAD-PEG10	L_d	0.690
12	KK114	HEAD-PEG10	L_o	0.395
13	KK114	HEAD-PEG50	L_d	0.690
14	KK114	HEAD-PEG50	L_o	0.393
15	Control with native lipids only	–	L_d	0.696
16	Control with native lipids only	–	L_o	0.412

2.2. Positioning of the dye depends significantly on the dye in question and its point of linkage to the host lipid

We first used atomistic simulations to determine the location of the lipid analogs inside the membrane bilayer, and specifically the location of the organic dye. To this end, the partial density profiles of the dye, lipids, and water molecules were calculated separately. For selected systems, they are depicted in Fig. 2 together with snapshots from the MD simulations showing representative locations and orientations of the dyes. For completeness, partial density profiles for all 14 systems that contained lipid analogs are shown in Figs. S1, S2, and S3.

The density plots demonstrate how the positioning of the different dyes is strongly dependent on the dye, the point of linkage, and also the membrane phase (Fig. 2, Figs. S1–S3). The cases shown in Fig. 2 demonstrate this with regard to the dye – the other variables remaining unchanged. While in Fig. 2 all the dyes are attached to the lipid headgroup, and all the membranes are in the L_d phase, the partitioning of the dyes can still be very different. ATTO647N (Fig. 2A,B) likes to reside in the membrane hydrophobic region, while ATTO532 (Fig. 2C,D) shares its time between the hydrophobic membrane region and the polar membrane-water interface. KK114 with a PEG10 linker (Fig. 2E,F), on the other hand, is only weakly bound to the membrane hydrophobic region and is instead located at the membrane-water interface and in the water phase.

A more detailed consideration reveals that, due to its hydrophobic nature, ATTO647N is predominantly located in the lipid phase in the hydrophobic core of a membrane, except when it is linked to a lipid headgroup in an ordered membrane environment (HEAD-L_o), where ATTO647N is distributed between the water and the lipid phases (Fig. S1). In this case, the headgroup attachment, in combination with the rigid and less permeable bilayer (L_o phase) makes snorkeling of the dye into the lipid phase less probable. In contrast, the highly polar dye ATTO532 strongly tends towards the water phase as highlighted, e.g., by the snapshot in Fig. 2B. ATTO532 is mainly in the water phase when it is linked to a lipid headgroup, as expected, however it is largely in the water phase also when linked to a lipid acyl chain (Fig. S2), introducing a considerable perturbation compared to the conformation of endogenous SM. Finally, for KK114 one observes partitioning between the lipid and water environments in all cases where it is attached directly to the lipid headgroup (Fig. S3A,B). Upon introducing a PEG linker in-

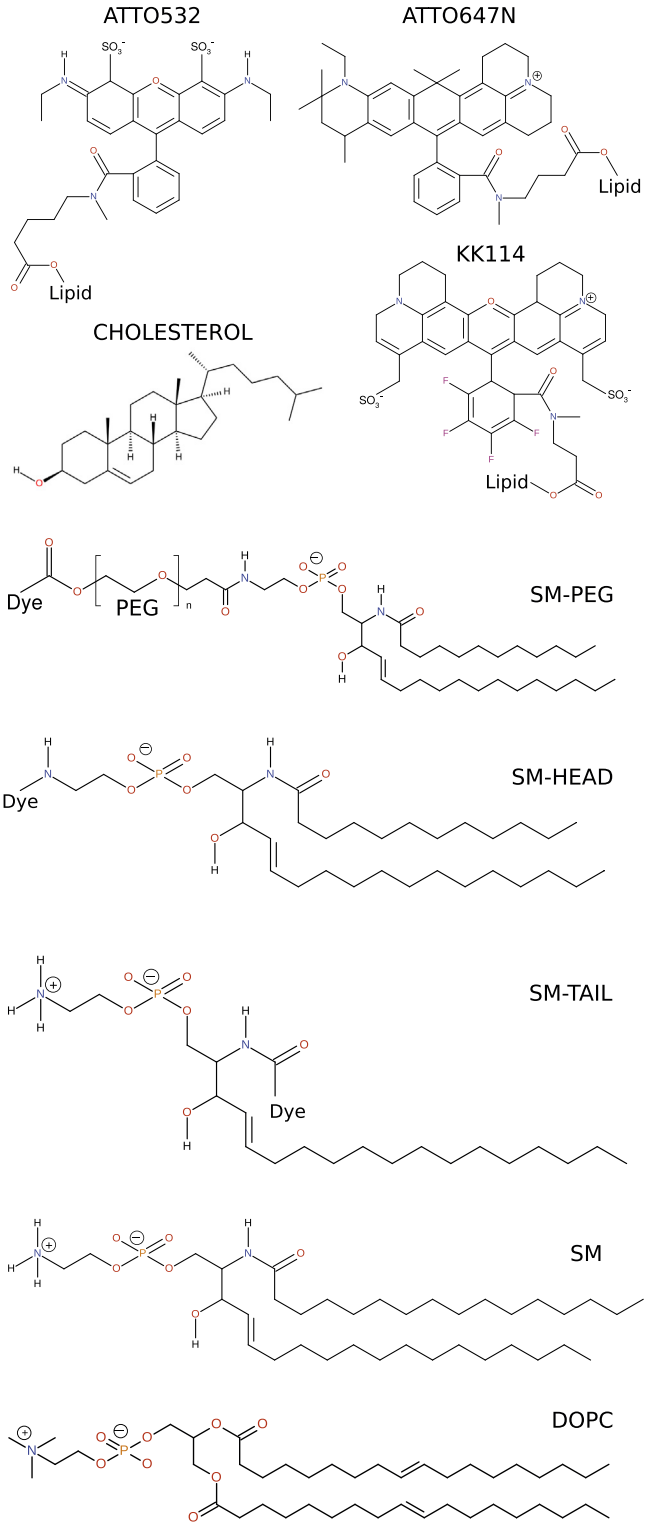

Fig. 1. Chemical structures of the dyes and lipids used in this study.

between KK114 and the lipid headgroup, in the L_o bilayer both the dye and the PEG linker reside in the water phase, while in the L_d bilayer the PEG chain has some affinity for the bilayer core (independently of its length) (Fig. S3). Yet the KK114 dye attached to the end of the chain spends most of its time in the water phase or at least above the polar lipid headgroup region, thus avoiding contact with the membrane hydrophobic core. Concluding, in all cases there is evidence that the dye interferes with membrane structure, however these effects are weakest

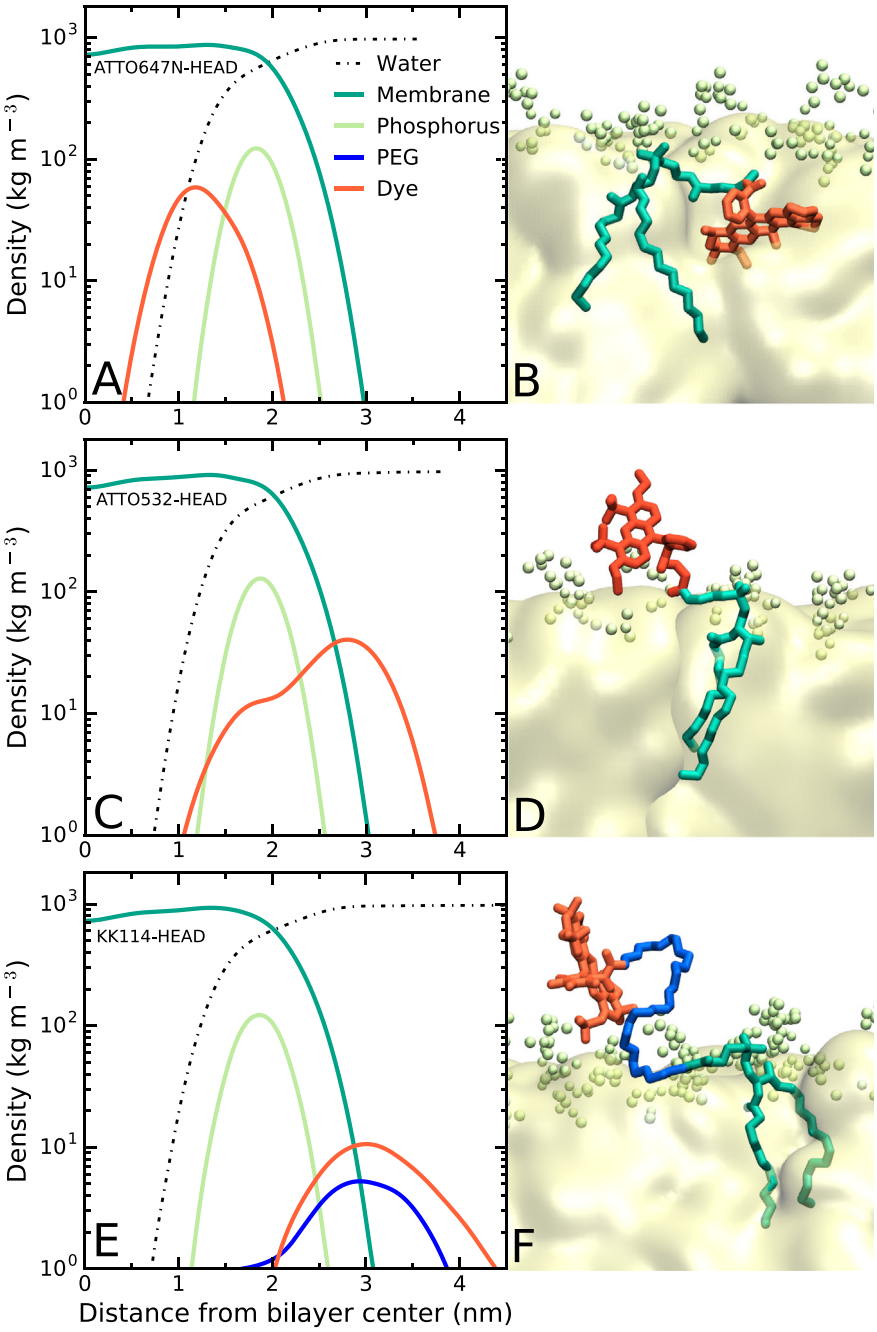

Fig. 2. Partial density profiles of the dye (red line), lipids (dark green line), lipids' phosphorus atoms (light green line), PEG linker (blue line), and water (dotted line) for (A) ATTO647N attached to a headgroup (HEAD) in a L_d bilayer; (C) ATTO532 attached to a headgroup (HEAD) in a L_d bilayer; and (E) KK114 attached to a headgroup (HEAD) via a PEG10 linker in a L_d bilayer. Representative snapshots of corresponding system structures are depicted on the right hand side: (B) ATTO647N (HEAD-L_d), (D) ATTO532 (HEAD-L_d), and (F) KK114 (HEAD-L_d via a PEG10 linker).

when the dye is attached to its host lipid via a long PEG linker.

2.3. Lipid analogs give rise to membrane perturbations, the weakest effects taking place with PEG-linked analogs

The positioning of the dye and the whole conformation of the lipid-dye pair may not only have an influence on the characteristics of the lipid analog itself but it will also affect the properties of the surrounding membrane environment. To estimate these effects we calculated two parameters from our simulations: the area per lipid (APL) and the deuterium order parameter (S_{CD}). The APL value is calculated by dividing the area of the simulation box in the membrane plane by the number of lipids in a single bilayer leaflet. An increase in APL consequently indicates that lipids are pushed away by the lipid analog and the lipid density adjacent to the lipid analog decreases. The observed values of APL (Table 1) are in the range of 0.69–0.74 nm^2 and 0.39–0.42 nm^2 for L_d and L_o bilayers, respectively. Table 1 lists the APL values determined for all 14 cases, including also a comparison to the unperturbed status, i.e. without a lipid analog (the last two rows of Table 1). The largest perturbations take place with ATTO647N-tagged SM lipids in the less ordered L_d environment, with the dye attached to the tail. This is not surprising since in this case the full integration of the dye into the bilayer leads to a large expulsion of lipids in its immediate environment. Interestingly, this expulsion is hardly present in the case

of the more ordered L_o environment, where the APL values hardly change relative to the unperturbed state. It seems that in a highly ordered membrane environment the lipids hardly give way, and the dye just integrates into the hydrophobic membrane region to fill the available free volume pockets. An increase in the APL values is also observed for ATTO532 in the L_d environment, where it partitions to a quite significant extent. Finally, only small changes in the APL values are generally observed for the KK114-labeled analogs. Integration of the PEG linker into the bilayer seems not to introduce a significant change in the membrane environment.

The deuterium order parameter S_{CD} is a measure of the orientation of a selected vector (C—D bond in this case) with respect to the bilayer normal. Values of S_{CD} were calculated according to the formula:

$$S_{CD} = \frac{1}{2} \langle 3 \cos^2 \theta_i - 1 \rangle \quad (1)$$

where θ_i is the angle between a C—D bond (C—H in simulations) of the ith carbon atom, and the bilayer normal. The angular brackets denote averaging over time and over relevant C—D bonds in the bilayer. In the extreme cases, the chains are either fixed in an all-trans conformation and rotate around the long molecular axis, where $S_{CD} = -0.5$, or the given bond rotates with a uniform distribution through all angles of space, leading to $S_{CD} = 0$.

Overall, we observed that $|S_{CD}|$ was inversely proportional to APL, as expected. Moving on, to determine the correlation length of structural perturbations induced by the dyes, we calculated profiles of the order parameter $|S_{CD}|$ for varying ranges of distance from the dye. To this end, let R stand for the radial in-plane distance (in 2D – using only the x,y coordinates of the molecules in the membrane plane) from the center of mass (COM) of a lipid acyl chain of a non-labeled lipid to the COM of a tail of the closest dye-tagged analog in the same membrane leaflet. Then, we determined separately the S_{CD} profiles of lipid acyl chains of i) lipids neighboring a dye ($R < 1.0$ nm), ii) lipids close to a dye ($1.0\,\text{nm} \le R \le 2.0\,\text{nm}$), iii) lipids farther away from the dye ($R > 2.0$ nm), and finally, as reference, also of iv) all lipids in an unperturbed bilayer (i.e., in reference systems without lipid analogs). Fig. 3 representatively depicts the S_{CD} profiles of ATTO532-TAIL in the L_d and L_o bilayers. The results for all the other profiles are shown in Figs. S4–S6.

The results allow us to draw several general conclusions. First, the structural perturbations due to the dyes are stronger in ordered membranes (L_o) than in more fluid bilayers (L_d). Second, tail-linked dyes induce stronger perturbations than headgroup-linked analogs. Third, the more hydrophobic the dye, the more significant are also the membrane perturbations. Finally, fourth, largely as a result of these three factors, the weakest dye-induced membrane alterations are observed in systems, where the dyes are attached to the headgroup of their host lipids by a PEG linker.

These findings are evident in particular among the lipids that are nearest neighbors to the dyes ($R < 1.0$ nm), since changes in S_{CD} can be quite significant in lipids that are in contact with the dyes. For increasing distance from the dyes, the effect of the dyes weakens rapidly and becomes largely negligible at distances beyond 2.0 nm, which is roughly three times the size of a lipid in the membrane plane.

In summary, in all cases the introduction of the lipid analogs leads to changes in the surrounding lipid bilayer, with the largest changes observed with the ATTO647N and ATTO532-tagged lipid analogs, particularly in the L_o phase, and the weakest changes observed with the PEG-linked KK114 lipid analogs.

2.4. Hydration of the dyes correlates with their ability to partition into the membranes

We next calculated the number of hydrogen bonds (H-bonds) formed between the dye and water molecules as well as between the dye and the lipids. A large number of H-bonds with water indicates strong hydrophilic characteristics and consequently stronger partitioning of the dye into the water phase, and vice versa into the bilayer. The values found in the simulations are listed in Tables S1–S3.

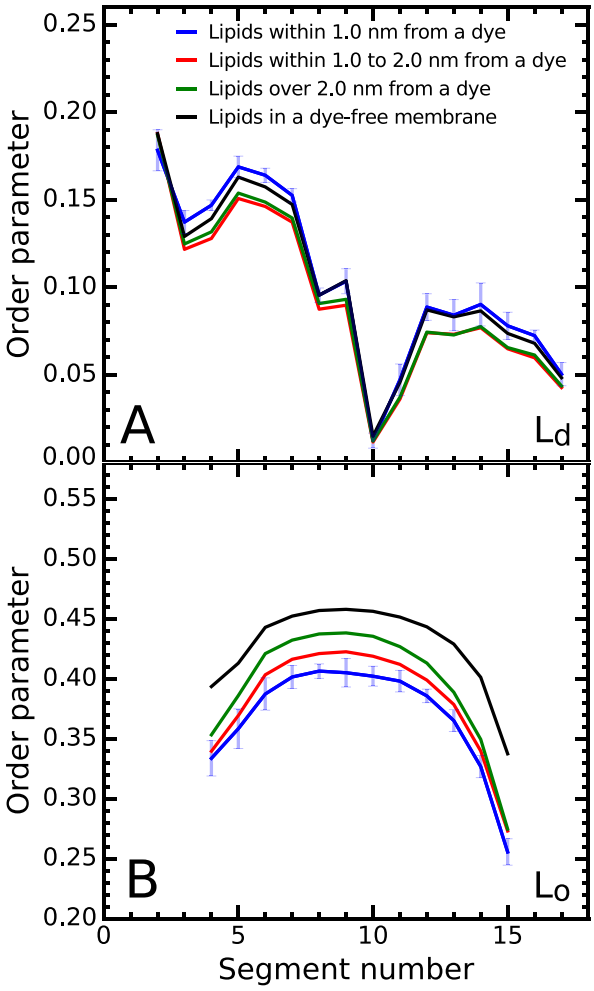

Fig. 3. Profiles of the $|S_{CD}|$ order parameter for ATTO532-TAIL and control systems in (A) L_d and (B) L_o phases (systems 7, 8, 15, and 16). The data have been calculated for the *sn*-1 chain of DOPC (in the L_d phase), and for the sphingosine chain of SM (in the L_o phase). Small segment numbers correspond to carbons in the acyl chain close to the headgroup; the largest segment number is the terminal carbon in the acyl chain. Results in both panels are given for i) lipids residing up to a distance of $R = 1.0$ nm from the closest dye-tagged analog (blue line), ii) lipids close to a dye ($1.0\,\text{nm} \le R \le 2.0\,\text{nm}$) (red line), iii) lipids far from the closest dye ($R > 2.0$ nm) (green line), and also for iv) all lipids in a dye-free bilayer (black line) used as a control. All data correspond to systems where ATTO532 is attached to an acyl chain (tail) of the host lipid.

On average there are about 2.0 H-bonds between ATTO647 and water. The small number is a clear sign of the hydrophobic nature of the dye and reflects the preference of ATTO647 to remain inside the membrane. For comparison, we found about 0.22 H-bonds between ATTO647 and lipids (data not shown). Meanwhile, for ATTO532 we identified on average 10.8 H-bonds with water. Again, for comparison, we found 0.44 H-bonds between ATTO532 and lipids (data not shown). Finally, for KK114 we found 14.5 H-bonds with water and 0.16 with lipids. One has to note the substantially larger size of KK114 in comparison to ATTO532 (38 carbon atoms in nonpolar groups for KK114 compared to 26 for ATTO532), thus ATTO532 is effectively more hydrated. Consequently, the revealed numbers of H-bonds with water are in strong agreement with the observed penetration of the dyes into the bilayers: the hydrophobic ATTO647 shows a higher preference for the membrane core, while ATTO532 and KK114 instead prefer the water

phase, with minor contacts with the membrane.

2.5. Microscopy results match simulation data: partitioning and diffusion are lipid analog dependent, highlighting some analogs to favor transient interactions that slow down lateral dynamics

Our MD simulations suggest that there are differences as to which membrane phase these lipid analogs prefer, i.e. the partitioning of the lipid analogs may differ from the one of unlabeled SM, which is thought to localize into ordered membrane environments [4]. In essence, based on our simulations, only KK114 attached to its host lipid via a PEG linker gives rise to membrane perturbations that are so minor in the L_o phase that the KK114-based SM analog could be expected to partition to the L_o phase in a manner similar to that of unlabeled SM. The other dyes induce stronger membrane perturbations, thereby disordering the membrane, and are likely to partition to the L_d phase.

We experimentally tested the order preferences of the different dye-tagged SM analogs using a biomimetic membrane system, i.e. giant plasma membrane vesicles (GPMVs) [32]. GPMVs are cellular-derived model membranes that preserve the cellular complexity to a large extent but do phase separate into more ordered (L_o) and disordered (L_d) environments [33]. Using the well-established fluorescence intensity read-out and its difference between L_o and L_d phases as well as data from a previous study [14], we calculated partitioning coefficients for the L_o phase (Fig. 4A); the smaller the value, the less the preference for the L_o environment. We used the same lipid analogs as in the simulations, with the only difference that a 45-unit long PEG linker (molecular weight of 2000) was employed instead of a 10 or 50-unit long linker chain used in the simulations, simply due to availability.

As can be observed from Fig. 4A, only the PEG-linked lipid analog experienced a significant preference for the L_o environment as expected for unlabeled SM. While also the ATTO532-tagged SM analogs showed reasonable L_o partitioning coefficients close to (but below) 50%, the ATTO647N (irrespective of HEAD or TAIL labeling) and KK114-HEAD lipid analogs showed minimal L_o preference (< 20%), as already highlighted before [14]. (Note that the KK114-TAIL SM analog was not available to us). These experimental data are in good agreement with the predictions given by our simulations that showed largest structural perturbations with ATTO647N and most minor alterations with the PEG-linked KK114 lipid analogs.

In the next step we experimentally investigated the influence of the dyes on the mobility and the diffusion modes of the labeled analogs in the plasma membrane of live PtK2 cells. Using STED-FCS we determined values of the apparent diffusion coefficients D_{conf} and D_{STED} for confocal (observation spot size d = 240 nm) and STED recordings (d = 50–80 nm, depending on the label), respectively. As highlighted before [10], D_{conf} gives an estimate of the overall macroscopic mobility, while $D_{rat} = D_{STED}/D_{conf}$ highlights the diffusion mode of the lipids, with D_{rat} = 1 indicating free Brownian diffusion and D_{rat} < 1 anomalous diffusion with trapping events arising from transient binding with slowly moving or even immobilized entities – the smaller the D_{rat} value, the stronger the interactions confining the motion.

The overall mobility (Fig. 4B) was similar for all analogs ($D_{conf} \approx 0.5\ \mu m^2/s$) except for ATTO532-TAIL, which was characterized by an increased overall mobility ($D_{conf} \approx 1.1\ \mu m^2/s$). Further, most of the SM analogs showed (Fig. 4C) strong trapping interactions ($D_{rat} \approx 0.2$), as highlighted before [9–11, 14], though expressing much weaker interactions for ATTO532-TAIL ($D_{rat} \approx 0.8$) [9, 14], and no or only weak interactions for KK114-PEG ($D_{rat} \approx 0.9$). It seems that for ATTO647N, ATTO532 (with the exception of ATTO532-TAIL), and KK114, the label does not influence the diffusivity of the lipid or its interactivity, despite the largely different conformations, environmental effects, and polarity (which is in accordance to previous studies, and also to results for other lipid analogs such as phospholipids and gangliosides [9, 10, 14, 31]. However, in the case of ATTO532-TAIL the very hydrophilic and polar dye loosens the membrane anchoring of the dye as revealed by increased mobility and decreased interactivity, highlighting less incorporation of the whole lipid analog. This decreased membrane anchoring of the ATTO532-TAIL analog in

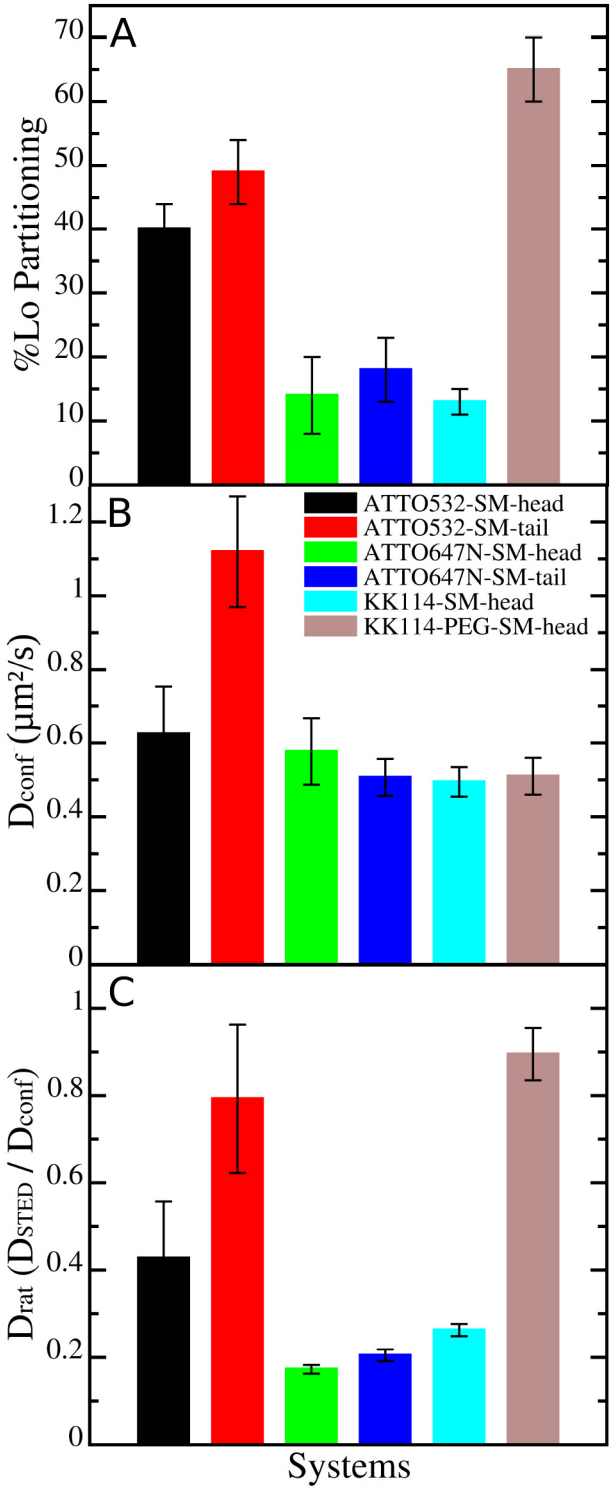

Fig. 4. Experimental results for the partitioning and diffusion behavior of the fluorescent lipid analogs. (A) Percentage of each lipid analog partitioning to the L_o phase. (B) FCS results for D_{conf} in $\mu m^2/s$ describing the macroscopic motion of lipid analogs (over large distances). (C) STED-FCS results for the ratio $D_{rat} = D_{STED}/D_{conf}$ describing whether the lipid analogs undergo transient binding events that slow down diffusion (D_{rat} < 1), or whether the diffusion process can be described by Brownian motion over both small and large spatial scales ($D_{rat} \approx 1$).

comparison to the other analogs has also experimentally been verified before through BSA washing experiments [9].

Surprisingly, the KK114-PEG SM lipid analog, despite its optimal characteristics concerning minimal membrane perturbation and accurate order preference, does not show the interactions observed with SM probes without the PEG linker. Rather this analog diffuses freely, the only explanation being the inert PEG linker, which builds a cloud-like cushion at the membrane-water interface (see also Fig. S3) and potentially weakens the integration into immobile protein assemblies (diffusion traps). However, the presence of a PEG linker does not generally interfere with SM-protein interactions to a significant degree, as shown in a recent study by Kinoshita et al. [34], who observed selected SM-based markers based on, e.g., ATTO594 attached to the host lipid via a hydrophilic glycol linker to recognize lysenin, a SM-specific binding protein. Further studies of KK114-PEG SM lipid analogs in a similar context with SM binding proteins would be useful but are beyond the present work and remain to be discussed elsewhere.

2.6. Diffusion of lipid analogs is dye-dependent and may deviate quite strongly from the diffusion of non-labeled host lipids

Experimental data show that the long-time lateral diffusion of lipid analogs is dye dependent and may lead to transient trapping. However, they do not bring up how strongly, if at all, the diffusion of lipid analogs differs from the diffusion of non-labeled host lipids. To clarify this matter, we analyzed the simulation data for lateral diffusion. For each lipid, we considered the diffusion of the lipid's center-of-mass in the 2D membrane plane and described its diffusion path as a series of lateral displacements over a time window of 1 ns each. The probability distribution function (PDF) of the lateral displacements resulted in the short-time lateral diffusion coefficient D (for details, see Materials and Methods).

The PDFs analyzed from the simulation trajectories are shown in Fig. S8 for both DOPC and the labeled lipids. Fig. S8 also shows the theoretical fits from which the values of D were obtained. The short-time diffusion coefficients found for the lipids in the L_d phase are of the order of 1–10 $\mu m^2/s$ and hence somewhat larger than in the regime of normal diffusion probed by the experiments. This is expected given that short-time diffusion is faster than long-time diffusion measured in experiments in the hydrodynamic limit.

The results shown in Fig. 5 describe the short-time diffusion coefficients of the lipid analogs scaled by the diffusion coefficient of the bulk lipid DOPC. If the ratio is around one, then the dye has little or no influence on diffusion. Meanwhile, a significant deviation from a value of one highlights a situation where the diffusion of the lipid analog differs from the diffusion of non-labeled lipids to a considerable degree. We find that the lipids labeled with ATTO532, especially in the head group, diffuse faster than DOPC, whereas ATTO647N slows down the diffusion of the labeled lipid regardless of the site of attachment. The KK114-labeled lipids diffuse similarly to DOPC, regardless of the presence and the length of the PEG linker. Curiously, the labeled lipids were not observed to perturb the dynamics of DOPC lipids in their immediate vicinity (data not shown).

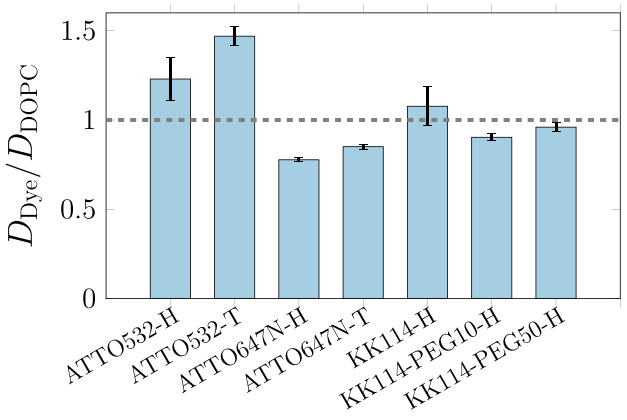

Fig. 5. Simulation results for the short-time lateral diffusion coefficients of the lipid analogs (D_{Dye}), shown relative to the corresponding lateral diffusion coefficient of the bulk lipid DOPC (D_{DOPC}). The horizontal dashed line is the reference for $D_{Dye} = D_{DOPC}$.

The behavior characterized by lateral diffusion is consistent with the above discussed partitioning of the dyes. As a hydrophobic dye, ATTO647N partitions largely to the membrane, thus slowing down its diffusion. ATTO532 in turn is a highly polar dye favoring the water phase, where diffusion is considerably faster than in the membrane, and over short time scales this difference is expected to increase the (short-time) diffusion. For KK114, the deviations from the lateral diffusion of DOPC are minor. Concluding, if the aim is to use lipid analogs to explore how non-labeled lipids diffuse in a membrane, then the results shown here suggest that KK114, preferably with a long PEG-linker attached to the head of the host lipid would be a reasonable choice.

3. Conclusions

Using atomistic MD simulations and microscopy experiments, we here showed the influence of an organic dye-tag on the structural characteristics, bilayer perturbations, membrane order preferences, and mobility of fluorescent lipid analogs. Specifically, we investigated sphingomyelin-based lipid analogs labeled at their acyl chain or headgroup with the organic dyes ATTO647N, ATTO532, and KK114, which differed in size and polarity. MD simulations highlighted that labels attached to a lipid chain have a larger perturbing effect on the membrane bilayer than labels attached to a headgroup. The more hydrophobic dyes were also found to perturb bilayer properties more than hydrophilic ones, mainly because they are located more in the lipid phase than in the water phase. Further, most of the analogs we studied turned out to have a higher tendency towards more disordered membrane environments, implying that they avoid ordered membrane regions that are typically strongly packed. This is partly surprising given that sphingomyelin used as the host lipid is thought to favor ordered membranes, and most of the lipid analogs we studied were based on dyes attached to the headgroup and favoring the water phase, where the influence of the dye on membrane properties is expected to be minor.

The simulation results are in agreement with experimental microscopy data on preferential partitioning of the sphingomyelin analogs into disordered membrane environments, overall highlighting a prominent positioning of the dye towards the membrane-water interface for both headgroup and acyl-chain labeling. Minimization of all these impacts on membrane properties was realized by the introduction of a PEG linker between the lipid headgroup and the dye. Importantly, despite the perturbations, all sphingomyelin analogs revealed in experiments a similar diffusivity in the cellular membrane with the same overall mobility and the same tendency to form transient interactions with less mobile entities. The congruence of the diffusion dynamics of the differently labeled analogs has similarly been shown for other lipid types such as phospholipids and gangliosides, and values the appropriateness of the observed lipid diffusion dynamics, whether investigated by (STED-)FCS [9–11] or other techniques. Exceptions are i) the analog labeled at the acyl chain with a very polar dye, which diffused much faster and showed a reduced affinity towards transient interactions, mainly due to a less tighter membrane anchoring, and which should consequently be avoided in fluorescence experiments; and ii) the PEG-linked lipid analog, which overall diffused similarly fast but showed no significant interactivity due to the inert PEG linker. These data suggest that the PEG linker enables proper investigations of the integration of the lipid analog into more ordered membrane environments (e.g. potential rafts) [11], but its usefulness to explore interaction

dynamics with other molecules associated with biological membranes should be clarified in more detail. Further, analysis of the lateral diffusion behavior observed in the atomistic simulations indicated that the short-time diffusion of lipid analogs was quite significantly different from the diffusion of the bulk lipid DOPC. KK114 was found to be an exception, however, in particular when it was linked to PEG, suggesting again that the use of a PEG-linker can minimize dye-induced effects on diffusion properties to a significant degree. Moving on, our experimental findings on the PEG-linked SM analog indicate that the trap-diffusion characteristics of the other SM analogs is independent of the partitioning characteristics between ordered/disordered domains in the plasma membrane, and that the PEG linker may shield the analog to become integrated into dense protein clusters (diffusion traps).

Our results highlight the strength of performing complementary in silico and super-resolution microscopy experiments. However, this study also highlights that great care has to be taken in terms of accurate controls when employing fluorescent lipid analogs, using, e.g., differently labeled analogs and observation techniques.

4. Materials and methods

4.1. Atomistic MD simulations

We performed atomistic simulations for 14 bilayer models with fluorescent moieties attached to lipids. Additionally, as controls, simulations for models of two dye-free membranes were also carried out. Every system was simulated three times as independent repeats. All studied systems are listed in Table 1.

Three fluorescent dyes were considered: ATTO647N, ATTO532, and KK114. The chemical structures of the dyes are shown in Fig. 1. These probes were attached to the headgroup of SM d17:1/12:0 or to the sphingosine chain as depicted in Fig. 1. Additionally, KK114 was also attached to a short 10 or 50 unit-long PEG linker via an ester group, while PEG was connected to the SM headgroup (Fig. 1).

The dye-lipid compounds were placed in two types of bilayers. The first bilayer was composed of 124 di-oleoyl-phosphatidylcholine (DOPC) molecules and 4 labeled lipids, representing the L_d phase. The second bilayer was composed of 42 cholesterol and 82 SM d18:1/16:0 molecules together with 4 labeled lipids, representing the L_o phase. The transmembrane distribution of each lipid type was symmetric. Bilayers were hydrated with about 6000 water molecules for systems without a PEG linker, and with about 30,000 water molecules for systems with PEG. Counter ions were included to neutralize the system.

All molecules were parameterized using the all-atom OPLS-AA force field [35]. In practice, we used OPLS-AA compatible lipid models derived from our previous studies [36–38]. Additionally, the PEG model was based on the OPLS-AA parameters and was validated in our previous studies [39]. For water, we used the TIP3P model [40]. For fluorescent labels, partial charges were calculated following the procedure used for lipids' parameterization [36]. In the first step of charge calculations the structures of the molecules were optimized using the second order Møller−Plesset perturbation theory, with the 6-31G** basis set. In the second step, the electrostatic potential around the molecules was calculated, and a polarizable continuum model was used to model the effect of aqueous environment [41]. In the third step, the partial atomic charges were calculated using the RESP program [42]. Calculated partial charges are given in SI as topology files used in the simulations. All quantum calculations were performed with the Gaussian09 package [43].

All MD simulations were performed with GROMACS v.5.0.4 [44]. All simulations were 400 ns long, where the first 200 ns were considered as equilibration. Simulations were performed with a time step of 2 fs. The LINCS algorithm was used to preserve bond lengths of other molecules [45], while SETTLE was used for water [46]. Simulations were performed at a constant temperature of 310 K and a pressure of 1 atm. Temperature was controlled via the Nose-Hoover thermostat with a time constant of 0.4 ps [47, 48]. The temperatures of water and the bilayer were controlled separately. Pressure was controlled by the semi-isotropic Parrinello-Rahman barostat [49]. Long-range electrostatic interactions were calculated with the smooth particle-mesh Ewald method [50, 51]. The Lennard-Jones interactions were cut off at 1 nm and dispersion correction was applied to both energy and pressure [52]. Altogether, the simulation program for 16 systems (Table 1) with 3 repeats each covered a time scale of about 19 μs.

4.2. Calculation of lipid short-time diffusion coefficients from the simulation trajectories

We analyzed lipid dynamics in terms of short-time diffusion coefficients, D, from 2D particle displacement data (describing the motion of each individual lipid in the membrane plane). The procedure to compute these diffusion coefficients is discussed below. This choice is justified by the small number of tagged lipids in the simulated systems, which renders calculation of the long-time diffusion coefficients — extracted from the mean-squared displacement data — quite unreliable. Moreover, since the diffusion in the L_o systems was slow, resulting in inadequate statistics for a reliable calculation of the diffusion coefficients, the short-time diffusion coefficients were determined only from the L_d phase membranes.

The lipid center-of-mass (COM) displacements in the membrane plane (r) over a time interval (Δ) of 1 ns were recorded, after the drift of the corresponding leaflet was eliminated. These displacements were binned in a histogram and normalized. This probability distribution function (PDF) $P(r,\Delta)$ was fitted with the theoretical prediction

$$P(r,\Delta) = \frac{r}{2D\Delta}\exp\left(-\frac{r^2}{4D\Delta}\right)$$

to find the diffusion coefficient D. For the PEG-linked dyes, we followed the COM of the membrane-spanning part up to the choline group. The values of D were calculated separately for DOPC and the tagged lipid in the two leaflets and in three simulation repeats. This provided six samples for both D_{DOPC} and D_{Dye}. We report the ratio D_{Dye}/D_{DOPC} as it is an appropriate figure of merit to describe whether the dynamics of the dye are similar to that of the host lipid DOPC. This ratio was extracted for each of the six pairs, and the mean value and standard error are reported.

Notably, diffusion over short time intervals is likely anomalous, which manifests itself as $D\Delta$ being replaced by $D_{eff}\,\Delta^{\alpha}$ with anomalous diffusion exponent α and effective diffusion coefficient D_{eff}. Unfortunately, the form of $P(r,\Delta)$ does not allow to distinguish between anomalous and normal diffusion, and hence the extracted values of D describe trends and the ballpark rather than absolute values that can be directly compared to experiment. Additional tests were carried out with other widths of the time window Δ, since with large values of Δ this analysis method would result in the long-time diffusion coefficient given by the mean-squared displacement analysis. We observed the trends and conclusions to be consistent with the values of Δ that we tested (1, 5, and 10 ns). However, the statistical fluctuations increased with increasing Δ, and with $\Delta = 10$ ns the PDF was not of sufficient quality for accurate fitting of D. The statistical fluctuations were not an issue with DOPC, but only with lipid analogs, since their number in the simulation systems was small, thereby rendering the sampling process quite challenging. For these reasons, the value of $\Delta = 1$ ns was chosen for the analysis.

4.3. Lipids and lipid analogs

We labeled SM either at the headgroup or at the lipid-water interface by replacing the native long acyl chain with a short acyl chain or a PEG(2000) linker carrying the dye, with different dyes (ATTO647N, ATTO532, or Abberior Star Red (KK114) [9, 14], whose synthesis has

been outlined in detail previously [9]. Fast DiO was purchased from Invitrogen (CA, USA).

4.4. Preparation of GPMVs

GPMVs were prepared as previously described [33]. In short, CHO cells were seeded out on a 60 mm petri dish in DMEM/F12 medium supplemented with 10% FBS. After two days (≈70% confluent), they were washed with a GPMV buffer (150 mM NaCl, 10 mM Hepes, 2 mM $CaCl_2$, pH 7.4) twice. 2 mL of GPMV buffer was added to the cells. 25 mM PFA and 10 mM DTT were added into the GPMV buffer. The cells were incubated for 2 h at 37 °C. Then, GPMVs were collected by pipetting out the supernatant.

4.5. Cell labeling

The PtK2 cells were grown in DMEM medium supplemented with 15% FBS. For labeling, they were incubated with 0.4 μM labeled lipid analog in a serum-free medium for 10 min. Then, the cells were washed a few times with PBS. 250 μL of cell media without phenol red was added onto the cells for imaging.

4.6. STED-FCS measurements

All STED-FCS data were taken by using a customized STED microscope [53]. The far-red dyes were excited using a 640 nm pulsed diode laser (Pico Quant), and fluorescence was depleted using a tunable far-red laser at 780 nm (Mai Tai). Fitting was performed with the FoCuS-point fitting program [54].

FCS data have been analyzed using standard fitting procedures as in detail described elsewhere [9–13], yielding values of the average transit time τ_D through the observation spot and thus of the apparent diffusion coefficient D. By recording FCS data for different intensities of the STED laser, we could determine those values for different sizes, i.e. diameters d of the observation spot sizes [9–13].

For calibration of the spot size $d(STED)$ at a certain STED laser intensity, measurements of the fluorescent lipid analogs in SLBs with different STED laser intensities were utilized [9–13]. Assuming free diffusion, the spot size calculation was done according to the following equation:

$$d(STED) = d(conf) \times \sqrt{\tau_{D(STED)} / \tau_{D(conf)}}$$

where $\tau_{D(conf)}$ and $\tau_{D(STED)}$ are the transit times measured for confocal (zero STED intensity) and at high STED laser intensity (varying for the different lipid analogs), respectively. The diameter $d(conf)$ of the confocal observation spots was determined by imaging 20 nm large fluorescent beads (green-yellow and crimson, Life Technologies).

The diffusion coefficient D was calculated from $\tau_{D(conf)}$ and $\tau_{D(STED)}$ according to:

$$D = \frac{d^2}{8 \times ln\,2 \times \tau_D}$$

For an evaluation of the diffusion mode, the confocal diffusion coefficient can be divided by the diffusion coefficient at the highest STED laser power yielding D_{conf}/D_{STED}.

Transparency document

The Transparency document associated with this article can be found, in online version.

Notes

Authors declared no conflict of interest.

Acknowledgments

For computational resources, we wish to thank the CSC–IT Center for Science (Espoo, Finland). This work was funded by the Academy of Finland (Center of Excellence in Biomembrane Research (grant no. 307415)) and European Research Council (Advanced Grant project CROWDED-PRO-LIPIDS (grant no. 290974)). ES is funded by EMBO Long term and Marie Skłodowska-Curie Intra-European (MEMBRANE DYNAMICS) postdoctoral fellowships. ES and CE are funded by Wolfson Foundation, the Medical Research Council (MRC, grant number MC_UU_12010/unit programmes G0902418 and MC_UU_12025), MRC/BBSRC/EPSRC (grant number MR/K01577X/1), and Wellcome Trust (grant ref. 104924/14/Z/14 and Strategic Award 091911 to the Micron Advanced Imaging Unit) for microscope facility usage and general lab and staff support.

Abbreviations

MD	molecular dynamics
L_d	liquid disordered
L_o	liquid ordered
PEG	poly-ethyl-glycol
DOPC	di-oleoyl-phosphatidylcholine
GM1	monosialotetrahexosylganglioside
STED	stimulated emission depletion
FCS	fluorescence correlation spectroscopy
KK114	Abberior Star Red
GPMVs	giant plasma membrane vesicles
SM	sphingomyelin

Appendix A. Supplementary data

Supplementary data to this article can be found online at https://doi.org/10.1016/j.bbamem.2018.07.003.

References

[1] K. Simons, Cell membranes: a subjective perspective, Biochim. Biophys. Acta 1858 (2016) 2569–2572.
[2] E. Sezgin, I. Levental, S. Mayor, C. Eggeling, The mystery of membrane organization: composition, regulation and roles of lipid rafts, Nat. Rev. Mol. Cell Biol. 18 (2017) 361–374.
[3] D. Lingwood, K. Simons, Lipid rafts as a membrane-organizing principle, Science 327 (2010) 46–50.
[4] K. Simons, E. Ikonen, Functional rafts in cell membranes, Nature 387 (1997) 569–572.
[5] T.S. van Zanten, S. Mayor, Current approaches to studying membrane organization, F1000Res. 4 (2015) 1380, https://doi.org/10.12688/f1000research.6868.1.
[6] L. Kastrup, H. Blom, C. Eggeling, S.W. Hell, Fluorescence fluctuation spectroscopy in subdiffraction focal volumes, Phys. Rev. Lett. 94 (2005) 178104.
[7] C. Eggeling, Super-resolution optical microscopy of lipid plasma membrane dynamics, Essays Biochem. 57 (2015) 69–80.
[8] E. Sezgin, Super-resolution optical microscopy for studying membrane structure and dynamics, J. Phys. Condens. Matter 29 (2017) 273001.
[9] C. Eggeling, C. Ringemann, R. Medda, G. Schwarzmann, K. Sandhoff, S. Polyakova, V.N. Belov, B. Hein, C. von Middendorff, A. Schonle, S.W. Hell, Direct observation of the nanoscale dynamics of membrane lipids in a living cell, Nature 457 (2009) 1159–1162.
[10] F. Schneider, D. Waithe, S. Galiani, J. Bernardino de la Serna, E. Sezgin, C. Eggeling, Nanoscale spatiotemporal diffusion modes measured by simultaneous confocal and stimulated emission depletion nanoscopy imaging, Nano Lett. 18 (2018) 4233–4240.
[11] A. Honigmann, V. Mueller, H. Ta, A. Schoenle, E. Sezgin, S.W. Hell, C. Eggeling, Scanning STED-FCS reveals spatio-temporal heterogeneity of lipid interaction in the plasma membrane of living cells, Nat. Commun. 5 (2014) 5412.
[12] F. Schneider, D. Waithe, M.P. Clausen, S. Galiani, T. Koller, G. Ozhan, C. Eggeling, E. Sezgin, Diffusion of lipids and GPI-anchored proteins in actin- free plasma membrane vesicles measured by STED-FCS, Mol. Biol. Cell 28 (2017) 1507–1518.
[13] V. Mueller, C. Ringemann, A. Honigmann, G. Schwarzmann, R. Medda, M. Leutenegger, S. Polyakova, V.N. Belov, S.W. Hell, C. Eggeling, STED nanoscopy reveals molecular details of cholesterol- and cytoskeleton-modulated lipid interactions in living cells, Biophys. J. 101 (2011) 1651–1660.
[14] E. Sezgin, I. Levental, M. Grzybek, G. Schwarzmann, V. Mueller, A. Honigmann, V.N. Belov, C. Eggeling, Ü. Coskun, K. Simons, P. Schwille, Partitioning, diffusion,

and ligand binding of raft lipid analogs in model and cellular plasma membranes, Biochim. Biophys. Acta 1818 (2012) 1777–1784.
[15] T. Baumgart, G. Hunt, E.R. Farkas, W.W. Webb, G.W. Feigenson, Fluorescence probe partitioning between L_o/L_d phases in lipid membranes, Biochim. Biophys. Acta 1768 (2007) 2182–2194.
[16] J. Juhasz, J.H. Davis, F.J. Sharom, Fluorescent probe partitioning in giant unilamellar vesicles of 'lipid raft' mixtures, Biochem. J. 430 (2010) 415–423.
[17] E. Sezgin, F.B. Can, F. Schneider, M.P. Clausen, S. Galiani, T.A. Stanly, D. Waithe, A. Colaco, A. Honigmann, D. Wüstner, F. Platt, C. Eggeling, A comparative study on fluorescent cholesterol analogs as versatile cellular reporters, J. Lipid Res. 57 (2016) 299–309.
[18] A. Honigmann, V. Mueller, S.W. Hell, C. Eggeling, STED microscopy detects and quantifies liquid phase separation in lipid membranes using a new far-red emitting fluorescent phosphoglycerolipid analogue, Faraday Discuss. 161 (2013) 77–89.
[19] R. Faller, Molecular modeling of lipid probes and their influence on the membrane, Biochim. Biophys. Acta 1858 (2016) 2353–2361.
[20] M. Kepczynski, T. Róg, Functionalized lipids and surfactants for specific applications, Biochim. Biophys. Acta 1858 (2016) 2362–2379.
[21] J. Repáková, J.M. Holopainen, M.R. Morrow, M.C. McDonald, P. Capková, I. Vattulainen, Influence of DPH on the structure and dynamics of a DPPC bilayer, Biophys. J. 88 (2005) 3398–3410.
[22] J. Repáková, J.M. Holopainen, M. Karttunen, I. Vattulainen, Influence of pyrene-labeling on fluid lipid membranes, J. Phys. Chem. B 110 (2006) 15403–15410.
[23] J. Curdová, P. Capková, J. Plásek, J. Repáková, I. Vattulainen, Free pyrene probes in gel and fluid membranes: perspective through atomistic simulations, J. Phys. Chem. B 111 (2007) 3640–3650.
[24] M. Franová, J. Repáková, P. Capková, J.M. Holopainen, I. Vattulainen, Effects of DPH on DPPC-cholesterol membranes with varying concentrations of cholesterol: from local perturbations to limitations in fluorescence anisotropy experiments, J. Phys. Chem. B 114 (2010) 2704–2711.
[25] M.D. Fraňová, J. Repáková, J.M. Holopainen, I. Vattulainen, How to link pyrene to its host lipid to minimize the extent of membrane perturbations and to optimize pyrene dimer formation, Chem. Phys. Lipids 177 (2014) 19–25.
[26] S. Rissanen, M. Grzybek, A. Orłowski, T. Róg, O. Cramariuc, I. Levental, C. Eggeling, E. Sezgin, I. Vattulainen, Phase partitioning of GM1 and its BODIPY-labeled analog determine their different binding to cholera toxin, Front. Physiol. 8 (2017) 252, https://doi.org/10.3389/fphys.2017.00252.
[27] K.C. Song, P.W. Livanec, J.B. Klauda, K. Kuczera, R.C. Dunn, W. Im, Orientation of fluorescent lipid analogue BODIPY-PC to probe lipid membrane properties: insights from molecular dynamics simulations, J. Phys. Chem. B 115 (2011) 6157–6165.
[28] M. Holtta-Vuori, R.-L. Uronen, J. Repakova, E. Salonen, I. Vattulainen, P. Panula, Z. Li, R. Bittman, E. Ikonen, BODIPY-cholesterol: a new tool to visualize sterol trafficking in living cells and organisms, Traffic 9 (2008) 1839–1849.
[29] A. Bunker, A. Magarkar, T. Viitala, Rational design of liposomal drug delivery systems, a review: combined experimental and computational studies of lipid membranes, liposomes and their PEGylation, Biochim. Biophys. Acta 1858 (2016) 2334–2352.
[30] C. Eggeling, A. Honigmann, Closing the gap: the approach of optical and computational microscopy to uncover biomembrane organization, Biochim. Biophys. Acta 1858 (2016) 2558–2568.
[31] V. Mueller, A. Honigmann, C. Ringemann, R. Medda, G. Schwarzmann, C. Eggeling, FCS in STED microscopy: studying the nanoscale of lipid membrane dynamics, Methods Enzymol. 519 (2013) 1–38.
[32] E. Sezgin, P. Schwille, Model membrane platforms to study protein-membrane interactions, Mol. Membr. Biol. 29 (2012) 144–154.
[33] E. Sezgin, H.J. Kaiser, T. Baumgart, P. Schwille, K. Simons, I. Levental, Elucidating membrane structure and protein behavior using giant plasma membrane vesicles, Nat. Protoc. 7 (2012) 1042–1051.
[34] M. Kinoshita, K.G.N. Suzuki, N. Matsumori, M. Takada, H. Ano, K. Morigaki, M. Abe, A. Makino, T. Kobayashi, K.M. Hirosawa, T.K. Fujiwara, A. Kusumi, M. Murata, Raft-based sphingomyelin interactions revealed by new fluorescent sphingomyelin analogs, J. Cell Biol. 216 (2017) 1183–1204.
[35] W.L. Jorgensen, D.S. Maxwell, J. Tirado-Rives, Development and testing of the OPLS all-atom force field on conformational energetics and properties of organic liquids, J. Am. Chem. Soc. 118 (1996) 11225–11236.
[36] A. Maciejewski, M. Pasenkiewicz-Gierula, O. Cramariuc, I. Vattulainen, T. Róg, Refined OPLS-all-atom force field for saturated phosphatidylcholine bilayers at full hydration, J. Phys. Chem. B 118 (2014) 4571–4581.
[37] W. Kulig, M. Pasenkiewicz-Gierula, T. Róg, Topologies, structures and parameter files for lipid simulations in GROMACS with the OPLS-AA force field: DPPC, POPC, DOPC, PEPC, and cholesterol, Data Brief 5 (2015) 333–336.
[38] T. Róg, A. Orłowski, A. Llorente, T. Skotland, T. Sylvänne, D. Kauhanen, K. Ekroos, K. Sandvig, I. Vattulainen, Package of GROMACS input files for molecular dynamics simulations of mixed, asymmetric bilayers including molecular topologies, equilibrated structures, and force field for lipids compatible with OPLS-AA parameters, Data Brief 7 (2016) 1171–1174.
[39] M. Stepniewski, M. Pasenkiewicz-Gierula, T. Róg, R. Danne, A. Orlowski, M. Karttunen, A. Urtti, M. Yliperttula, E. Vuorimaa, A. Bunker, Study of PEGylated lipid layers as a model for PEGylated liposome surfaces: molecular dynamics simulation and Langmuir monolayer studies, Langmuir 27 (2011) 7788–7798.
[40] W.L. Jorgensen, J. Chandrasekhar, J.D. Madura, R.W. Impey, M.L. Klein, Comparison of simple potential functions for simulating liquid water, J. Chem. Phys. 79 (1983) 926–935.
[41] M. Cossi, G. Scalmani, N. Rega, V. Barone, New developments in the polarizable continuum model for quantum mechanical and classical calculations on molecules in solution, J. Chem. Phys. 117 (2002) 43–54.
[42] C.I. Bayly, P. Cieplak, W. Cornell, P.A. Kollman, A well-behaved electrostatic potential based method using charge restraints for deriving atomic charges: the RESP model, J. Phys. Chem. 97 (1993) 10269–10280.
[43] M.J. Frisch, G.W. Trucks, H.B. Schlegel, G.E. Scuseria, M.A. Robb, J.R. Cheeseman, J.A. Montgomery Jr., T. Vreven, K.N. Kudin, J.C. Burant, et al., Gaussian 03, Revision C.02, Gaussian, Inc., Wallingford, CT, 2004.
[44] M.J. Abraham, T. Murtola, R. Schulz, S. Páll, J.C. Smith, B. Hess, E. Lindahl, GROMACS: high performance molecular simulations through multi-level parallelism from laptops to supercomputers, SoftwareX 1-2 (2015) 19–25.
[45] B. Hess, H. Bekker, H.J.C. Berendsen, J.G.E.M. Fraaije, LINCS: a linear constraint solver for molecular simulations, J. Comput. Chem. 18 (1997) 1463–1472.
[46] S. Miyamoto, P.A. Kollman, Settle: an analytical version of the SHAKE and RATTLE algorithm for rigid water models, J. Comput. Chem. 13 (1992) 952–962.
[47] S. Nosé, A unified formulation of the constant temperature molecular dynamics methods, J. Chem. Phys. 81 (1984) 511–519.
[48] W.G. Hoover, Canonical dynamics: equilibrium phase-space distributions, Phys. Rev. A 31 (1985) 1695–1697.
[49] M. Parrinello, A. Rahman, Polymorphic transitions in single crystals: a new molecular dynamics method, J. Appl. Phys. 52 (1981) 7182–7190.
[50] T. Darden, D. York, L. Pedersen, Particle mesh Ewald: an N log(N) method for Ewald sums in large systems, J. Chem. Phys. 98 (1993) 10089–10092.
[51] U. Essmann, L. Perera, M. Berkowitz, A smooth particle mesh Ewald method, J. Chem. Phys. 103 (1995) 8577.
[52] M.R. Shirts, D.L. Mobley, J.D. Chodera, V.S. Pande, Accurate and efficient corrections for missing dispersion interactions in molecular simulations, J. Phys. Chem. B 111 (2007) 13052–13063.
[53] S. Galiani, D. Waithe, K. Reglinski, L.D. Cruz-Zaragoza, E. Garcia, M.P. Clausen, W. Schliebs, R. Erdmann, C. Eggeling, Super-resolution microscopy reveals compartmentalization of peroxisomal membrane proteins, J. Biol. Chem. 291 (2016) 16948–16962.
[54] D. Waithe, M.P. Clausen, E. Sezgin, C. Eggeling, FoCuS-point: software for STED fluorescence correlation and time-gated single photon counting, Bioinformatics 32 (2016) 958–960.
[55] B. Hess, Determining the shear viscosity of model liquids from molecular dynamics simulations, J. Chem. Phys. 116 (2002) 209–217.